Fractional Order PI Control in Hybrid Renewable Power Generation System to Three Phase Grid Connection

Ali Mohamed Yousef[1], Farag K. Abo-Elyousr[1], Ahmed Elnozohy[1], Moayed Mohamed[2] and Saad A. Mohamed Abdelwahab[3]

[1] Electrical Engineering Department, Faculty of Engineering, Assuit University, Assuit, Egypt.
[2] Electrical Department, Faculty of Technology and Education, Sohag University, Sohag, Egypt.
[3] Electrical Department, Faculty of Technology and Education, Suez University, Suez, Egypt.
drali_yousef@yahoo.com, eng_farag_k_usr@yahoo.com, ahmed.alnozahy@gmail.com, moayedm1990@gmail.com, saad.abdelwahab@suezuniv.edu.eg

Abstract: The main objective of this paper is to allow renewable energy sources (RES) to actively participate within hybrid microgrid by proposing a new control system based on fractional order proportional integral (FOPI) controller. Fractional order proportional integral controller is a classical proportional integral (PI) in which the integral part is a fraction instead of integer numbers. The paper introduces a hybrid photovoltaic (PV), wind turbine and battery storage system connected to a three-phase grid. Three types of controller are considered and compared for a hybrid renewable energy system (HRES), namely, FOPI, PI, and the fractional order integral control (FIC). For the PV resource, maximum power point tracking (MPPT) controller was designed using the incremental conductance plus integral regulator technique. A DC/DC boost converter was utilized to connect the renewable energy resources to a point of common coupling. MATLAB/Simulink is adopted to perform the simulation results of the developed HRES. The results show that the FOPI controller outperforms other controllers under several operating conditions. The paper also includes experimental results from a prototype real scale.

Keywords: photovoltaic, fractional order proportional integral, hybrid renewable energy system, maximum power point tracking, voltage source control, three-phase grid.

1. Introduction

Because of environmental problems and energy crises, clean and renewable energy generation resources are important priorities by many governments around the world and among the most widespread renewable energy are solar and wind energy [1]. Renewable energy sources (RES) have been filtered to solve problems related to the increasing demand for electrical loads and the environmental side effects of traditional fossil fuel sources that cause numerous damages to humans and society, which are mainly used in conventional power plants [2]. The increasing trend of renewable energy is in response to the harmful environmental impacts of increased carbon emissions for conventional power plants and increased electrical loads worldwide [3], [4].

The most common components in hybrid renewable energy systems (HRESs) are the PV, wind turbine and battery storage. Normally, these three types of resources are connected together via the DC-DC converters. A DC-DC converter transforms the DC energy to an appropriate DC level at the point of common coupling, which is a compulsory step for grid connected AC three-phase inverters. The HRES combines several renewable resources, which is deemed to be a solution to avoid the problems of dependence on a single resource [5] to meet load demands or transfer such renewable energy to a three-phase grid. All these resources are connected in parallel to supply the energy demands [6]. Normally, maximum power point tracking techniques (MPPT) are employed to significantly enhance the efficiency of the PV modules and wind-turbine systems [7]. However, there has been an increase in the number of resources which are DC in nature, or whose ac frequency is neither constant nor match the utility grid frequency. In some of these cases, three-phase inverters have been used. Besides, a control of both active and reactive powers is provided in order to deliver the electrical energy with the same utility grid frequency [8].

Received: October 1th, 2019. Accepted: June 6th, 2020
DOI: 10.15676/ijeei.2020.12.3.5

With the above challenges, the authors of this work are motivated to develop modern controllers thereby regulating the energy transferred by voltage source inverter (VSI). In its many applications of fractional differentiation and integration, science and engineering branches use many fractional derivatives. The most widely used in research are Caputo and Riemann-Liouville derivatives, which have been widely used in modeling complex dynamics that appear in physics, biology, engineering, and many other fields [9].

The fractional order proportional integral (FOPI or PIλ) controller has been a topic of interest of researchers from academia and industry in the last years. They are more flexible and provide improved performance than conventional PI controllers [10] rather than the basic characteristics of the PI adapted on the power systems [11,12]. In the literature, the fractional-order PI (FOPI) and integral controllers were being investigated. In [13], F. K. Abo-Elyousr et al (2019) has developed an FOPI controller, which renders multiple poles and zeros in the designing procedures, to solve load frequency issues regarding massless inertia resources. The authors of [13] demonstrated that FOPI controller had outperformed the other controllers. In another research [14], A. Kumar (2020) et al utilized a fractional derivative with particle swarm optimization to design a finite impulse response. V. A. Kumar et al (2020) have investigated fractional order controller for cascaded islanded H-bridge [15]. In another article [16], fractional order PID was introduced to enhance the stability of HVDC system. A. Narendran et al (2020) conducted a research to design an inverter fed induction motor whereby the fractional order controller demonstrated a competitiveness amongst the other controllers [17]. A. Rawat et al (2020) conducted a research to employ FOPID for PVs maximum power point tracking [18]. In another research [19], a fractional order PI was utilized to control the pitch angle of wind turbines. B. Puschalski et al (2020) conducted a research via fraction order PID together with fuzzy controller for a pressurized water type nuclear reactor with a conclusion that fractional order controllers have strong efficacy [20]. The investigation of the above manuscripts reveals that fractional order controllers are limited in the literature regarding HRES based grid connected inverters, which gives the authors another motivation to develop fractional order-based controllers.

At the level of servo systems, Z. Qi et al (2019) conducted a research to design a FOPID and concluded that FOPID has better performance [21]. In another article [22], F. Meng et al (2020) introduced fractional order PID to control a motor torque and demonstrated that fractional order controllers had better performance. A survey for fractional order controllers was conducted in [23]. A design algorithm for fractional controllers combined with fuzzy was conducted by J. Z. Shi with a conclusion that fractional controllers had proven better performance (2020) [24]. Fractional order was utilized by Zaheeruddin et al (2020) at the level of hybrid microgrid to design a load frequency controller [25]. In another article [26], R. P. Kumar et al (2020) introduced a FACT based on fractional order PID with PQ coordination theory for a grid connected RES and showed that FOPID had surpassed the other developed controllers regarding the power quality issues. In [27], fractional order controllers were utilized for an air heating system. In [28], fractional order PID controller based fuzzy was employed to fix to mitigate the vibration isolation for a meteorological elastomer. A. K. Patra et al. (2020) introduced a fractional order PID for a suspension vehicle [29]. Fractional order controllers were adopted by by M. S. Bouakkaz to help enhance the PV generation [30].

Despite the rich literature survey of fractional order in several fields, yet, the application of fractional order controllers for grid connected HRES is rare. For such challenging tasks, the paper contributes in the literature as (i) to develop a fractional order PI (FOPI) controller, (ii) the effectiveness developed FOPI is verified through a fair comparison with the classical and integral order PI, and fractional order integral controllers, (ii) considering the changeable conditions of PV (irradiance and temperature) and wind turbine (wind speed) of the system.

The remaining of this paper is organized as follows, system description and proposed controllers are introduced in sections 2 and 3. The simulation results and discussions are given in section 4. The experimental results and conclusions are given in sections 5 and 6, respectively.

2. System Description

The HERS generation system proposed in this paper as shown in Figure 1. The proposed system consists of a wind generation, PV system, energy storage, boost converter, DC link, three-phase inverter, controller, high transformer, and the utility grid and AC loads. Normally, a VSI inverter is employed to change form the DC side to the grid the utility grid side.

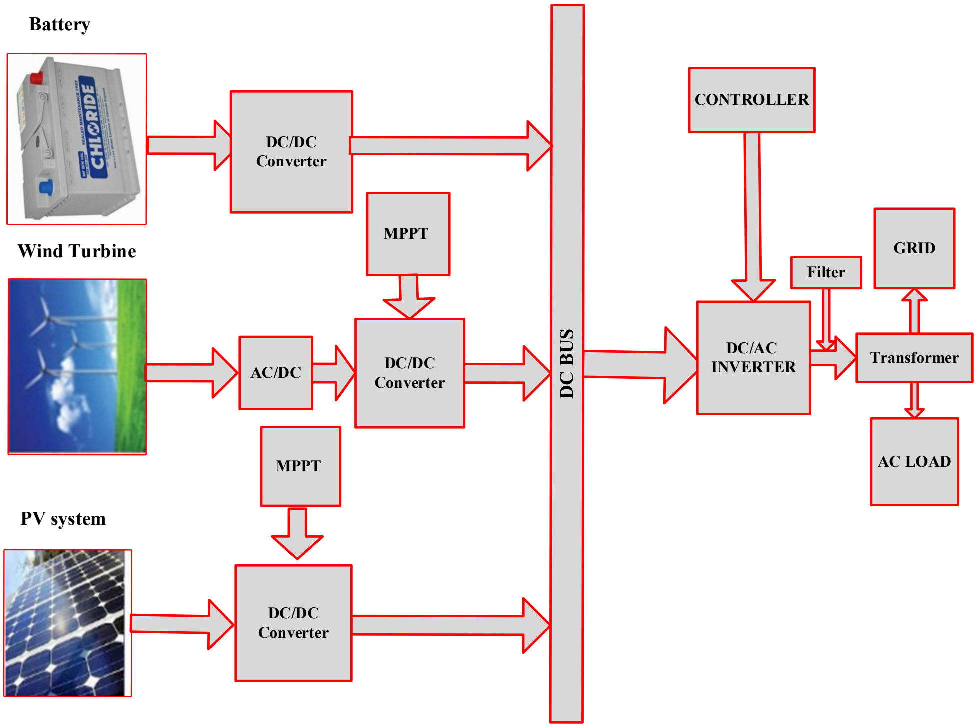

Figure 1. Hybrid renewable energy generation system configuration.

A. PV System

Electrical Energy is used to customers, Converters are used to convert the PV energy which come from sun light into continuous electrical energy [3]. Modeling and simulation have a very important role for solar cells in designing true simulation of PV modules [30]-[31].

The equation of output voltage from PV describes the voltage root mean square (rms), which is being provided by the PV module voltage (V_{dc}).

$$V_{rms} = 0.612\, M_a V_{dc} \tag{1}$$

Mathematical modeling of solar cells is an important step in the analysis and design of photovoltaic control systems. The photoelectric mathematical model can be obtained from the following equations: The equation that describes the "current-voltage" of the PV cell is given as:

$$I_c = I_{ph} - I_o \left\{ e^{\left[\frac{q}{AkT}(V_c + I_c R_s)\right]} - 1 \right\} \tag{2}$$

$$V_c = \frac{AkT}{q} \ln\left(\frac{I_{ph} + I_o - I_c}{I_o} \right) - I_c R_s \tag{3}$$

$$I = I_{ph} - I_o \left\{ e^{\left[\frac{q}{n_s AKT}(V + n_s IR_s)\right]} - 1 \right\} \tag{4}$$

$$V = \frac{n_s AkT}{q} \ln\left(\frac{I_{ph} + I_o - I}{I_o} \right) - n_s IR_s \tag{5}$$

Where;

$$I_{ph} = \frac{G}{1000}[I_{sc} + k_i(T - T_r)] \tag{5a}$$

$$I_o = I_{or}\left(\frac{T}{T_r}\right)^3 e^{\left[\frac{qE_g}{AK}\left(\frac{1}{T_r} - \frac{1}{T}\right)\right]} \tag{5b}$$

The module output power could be detected simply as in (6).

$$P = VI \tag{6}$$

The PV cell equivalent circuit is shown in Figure. 2. From the PV model, the I-V curve and P-V curve in Figure.3. The incremental conductance plus integral regulator technique is utilized to find the global MPPT of the PV module.

Where, P is output PV power, I is output PV current, V_c is cell PV voltage (V), I_o is diode current (A), I_{or} is diode saturation current (A), V is diode voltage (V), K is constant of boltzmann = 1.3806*10-23 J.K-1, n1 is diode factor of ideality up to 1.0, q is charge of electron = 1.6022*10-19, G is solar radiation and T is cell temperature (Co).

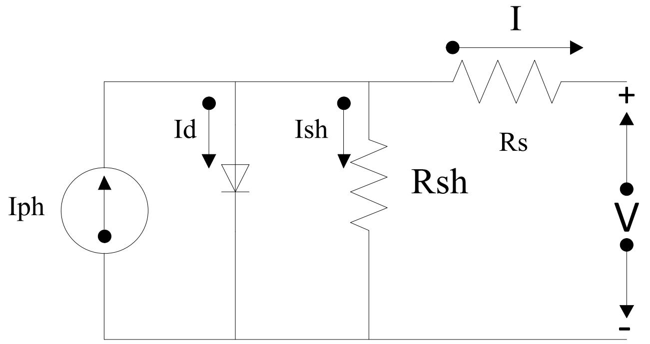

Figure 2. PV cell equivalent circuit.

B. Wind Turbine

The generator can optionally be a synchronous or asynchronous generator. Variable speed wind turbines are used with a full-range power transformer with a permanent magnetic synchronous generator (PMSG). PMSG is one of the most used types in wind energy because it is characterized by more gravity in wind energy applications because of its nature in using permanent magnets to obtain magnetic field instead of winding, which causes copper losses [32]. This configuration is compatible with the changing wind turbines with full speed generator connected to the network through a full-scale frequency converter [33]. Wind speed is the important factor for determining the power of wind turbines. In this research was used PMSG [34]. For system design and control, the need for dynamic modeling of a wind energy conversion system is required in this paper. Wind energy is obtained from the kinetic energy (E) given by equation (7). In order for wind energy to be obtained by distinguishing kinetic energy in the wind as shown in equation (8). In equation (9), the wind mass flow rate for obtaining electrical energy is discipled. By replacing equations (9) in (8), wind energy can be expressed as in (10).

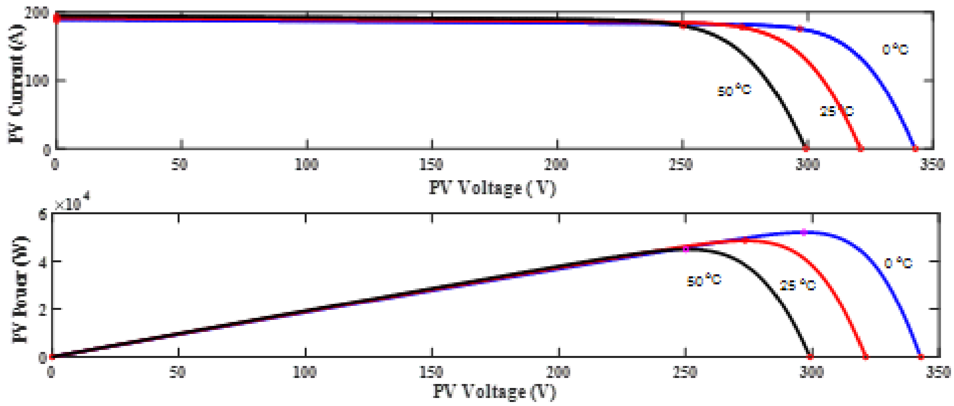

(a)

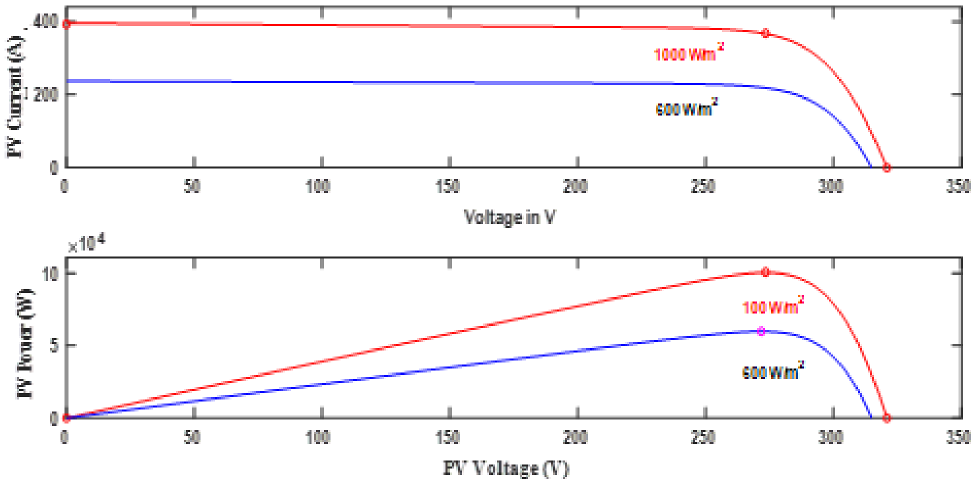

(b)

Figure 3. PV output characteristics I-V and P-V curves at (a) different temperature, (b) different irradiation.

$$E = \frac{1}{2}\dot{m} * V^2 \tag{7}$$

$$P = \frac{dE}{dt} = \frac{1}{2}\dot{m} * V^2 \tag{8}$$

$$\dot{m} = \rho A v \tag{9}$$

$$p = 0.5\,\rho A v^3 \tag{10}$$

The calculation of the actual mechanical capacity to generate the wind energy harvested from wind turbines can be obtained as in equation (11). Besides, the mechanical torque is given as in (12).

$$P_m = \frac{1}{2}\,\rho\pi R^2 C_p V^3 \tag{11}$$

$$T_m = \frac{P_m}{w_m} \tag{12}$$

Most PMSG properties are similar to the synchronous generator used in wind energy generation. The mathematical model equation voltages of the machine are calculated in (13).

$$\boldsymbol{V_{dq0} = K_{CP} V_{abc}} \tag{13}$$

The tip speed ratio of a wind turbine can be calculated in (14). Figure 4 shows a typical C_p versus λ_r curve for PMSG of wind turbine.

$$\lambda_r = \frac{w_m R}{V_w} \tag{14}$$

Where; V_d ,V_q represents the stator voltages in the d-q axis respectively, ω_s is the angular velocity of the synchronously rotating reference frame, $\boldsymbol{C_p}$ is the power coefficient, $\boldsymbol{P_m}$ is mechanical power, ṁ is the air mass, v is the wind speed, $\boldsymbol{\rho}$ is the density of air, A is the rotor blade area and R the wind turbine rotor radius. The $\boldsymbol{C_p}$ is related to and tip speed ratio (λr), Tm is mechanical torque (N.m), VW is the wind speed (m/s), β is pitch angle of blades (deg), ωr is the wind turbine rotational speed (rad/s).

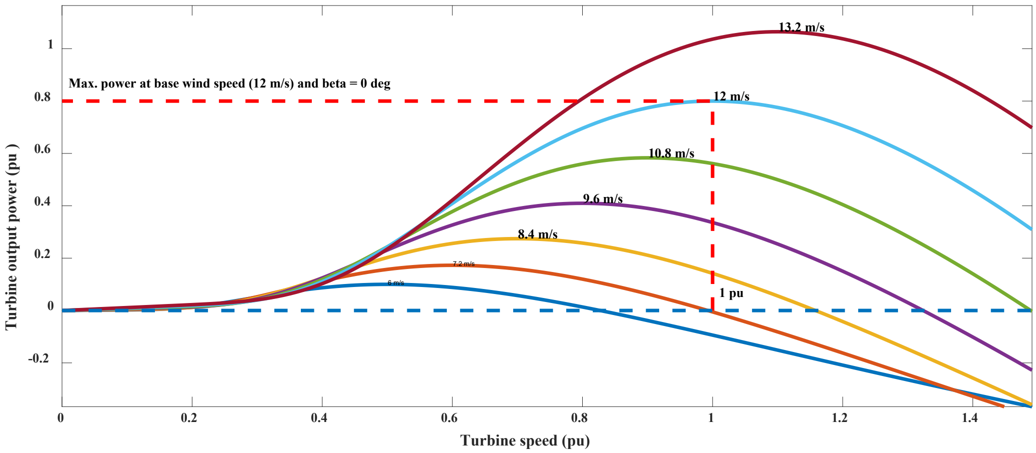

Figure 4. A typical C_p versus λ_r curve.

C. Battery Storage

Battery storage is important part of the system HREs. Electrical energy generated from renewable sources depends entirely on weather conditions such as wind speed and variable sunlight throughout the day, which enhances the use of energy storage necessary with it. [35]. Power Storage is the key concerns worldwide when developing the HRES. If conditions are bad the power from the system to grid is low, here battery play important role to give the energy [36]. Herein, Ni-MH connected to a DC-DC boost converter is utilized. Because intermittent nature of renewables, a battery storage is utilized to meet the power demand to the grid and the local loads.

Electric energy generated from renewable sources depends on changing weather conditions such as wind speed and sunlight. Power Storage is the key concerns worldwide when developing the HRES [28]. PV panels work in sun light at all days and wind turbine work in all the best of time the conditions allow to it. Because intermittent nature of renewables, A battery storage is utilized to get the power demand to the grid and the loads connect with the system. The type of the used battery is Ni-MH battery connected to a DC-DC boost converter.

D. DC-DC Converter

In this system authors used the type of DC-DC Converter is Boost converter to set up voltage level. The maximum power from the HRES voltage level is raised to a suitable level, then transferred to the three-phase inverter and to the grid or AC load through DC-DC converter [37]. The output voltage can be expressed as the next equation. the topology of boost converter as shown in Figure 5.

$$Vo = \frac{Vs}{1-D} \tag{15}$$

Where, V_S is converter input voltage (V), V_O is boost converter output voltage (V) and D is duty cycle of the boost converter.

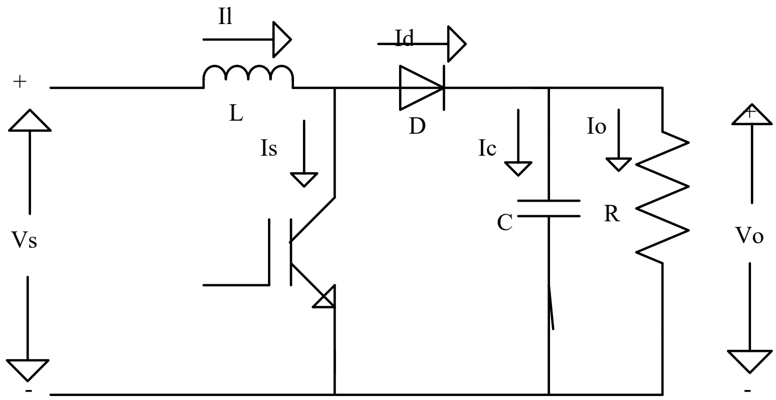

Figure 5. DC-DC Boost Converter.

3. Proposed controllers

A new approach is used to control the three-way switch to improve the performance of the networked HRES system. As shown in Figure. 6, it uses four steps at the same time of control: the first control loop, which is a process that regulates the AC voltage which controls the size of the AC voltage from VSI, and the second is the constant voltage of the capacitor DC which is the DC voltage regulator which is the preservation On the output voltage of VSI. The third and fourth controls for regulating the volume and phase of the VSI output current at appropriate values under different operating conditions in the wind and solar radiation to maintain the inverter output power factor in the unit operation. [38].

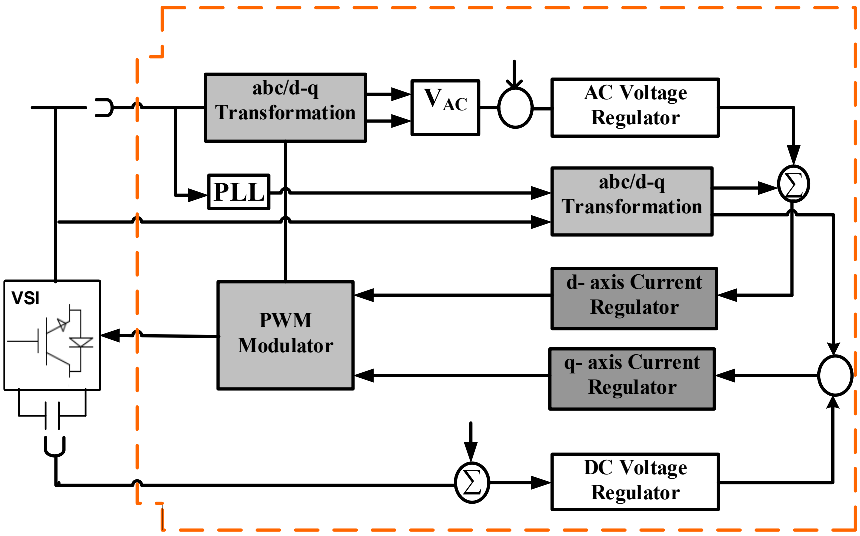

Figure 6. Block of controller in inverter of the system.

A. Classic Proportional Integral Controller (PI)

PI control is still the most popular feedback design in industry. The PI controller has two constant parameters K_p for proportional and K_i for integral term [39]. The operating logic of the PI controller considers the optimum technique to be used in HRES. The summation of two terms adjusts the process through a control element as in (16).

$$G(s) = K_p + \frac{K_i}{s} \tag{16}$$

Where, Kp is a proportional control, Ki is an integral control and G(s), is the functions of the variable s.

The goal of the integrated terminology of the PI controller is to have a stable state error of zero for step input in long-term operating conditions [40], [41]. Figure. 7 demonstrates a schematic diagram of the internal structure of the PI block.

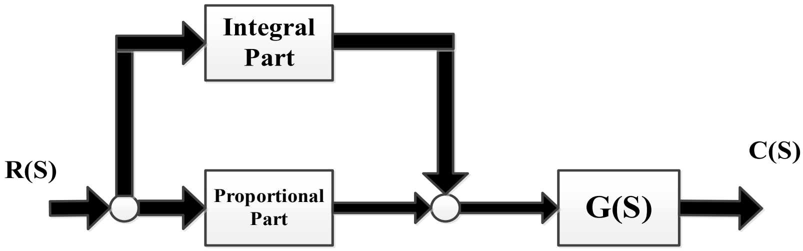

Figure 7. Internal structure of PI block

B. Integral Control (IC)

The IC parameters depend on non-integer-order fundamental operator, $_aD_t^{\alpha}$, where a and *t* are the bounds of operation and α ϵR [42]. The continuous integral operation is defined as (17).

$$_aD_t^{\alpha} = \left\{ \begin{array}{ll} \frac{d^{\alpha}}{dt^{\alpha}}: & \alpha > 0, \\ 1 \quad : & \alpha = 0, \\ \int_a^t (dT): & \alpha < 0. \end{array} \right\} \tag{17}$$

Where, $_aD_t^{\alpha}$ is a a generalization of integration and differentiation to non-integer-order fundamental operator, the components a and t are bounds of operation.
The important function used in fractional integral is called gamma function, which is defined as:

$$\Gamma(n) = \int_0^{\infty} t^{n-1} e^{-t} dt. \tag{18}$$

This function is a generalization of the factorial in the following from:

$$\Gamma(n) = (n-1)! \tag{19}$$

Where, Γ is the gamma function is directly implemented in MATLAB with syntax

C. Fractional Order PI Control (FOPI)

From the control methods, fractional order PI^{λ} controller was introduced as a generalization of the classical PI controller [42]. Generally, FOPI is a classic PI whereby the integral order of the Laplace's operator is a fraction rather than integer.

Several partial differentiation definitions have been suggested thereby the most common among them is the definition of Riemann-Liouville (R-L), the definition of Grunwald-Letnikov (G-L) [43]. The following equations show the basics of fractional calculus.

1- The Riemann-Liouville (R-L) definition is given as in (20).

$$_aD_t^{\alpha}f(t) = \frac{1}{\Gamma(n-\alpha)} \frac{d^n}{dt^n} \int_a^t \frac{f(\tau)}{(t-\tau)(\alpha-n+1)} d\tau, \tag{20}$$

Where, *f* (t) is a function assumed to be sufficiently smooth and locally integrable and Γ(.) is the gamma function for (n − 1 < α < n).

2- The Grunwald-Letnikov (G-L) definition

$$ {}_{a}D_{t}^{\alpha}f(t) = \lim_{h \to 0} h^{-\alpha} \sum_{j=0}^{\left[\frac{t-a}{h}\right]} (-1)^{j\alpha} C_j \, f(t - jh), \quad (21)$$

where, αC_j is a binomial coefficient.

3- The Caputo definition is given as

$$ {}_{a}D_{t}^{\alpha}f(t) = \frac{1}{\Gamma(n-\alpha)} \int_{a}^{t} \frac{f^{n}(\tau)}{(t-\tau)^{(\alpha-n+1)}} d\tau. \quad (22)$$

Among the aforementioned three definitions, the most commonly used is the Riemann-Liouville (R-L) definition. The R-L definition and Caputo definition are almost the same except for some initial value settings [44, 45]. The Laplace transform under zero initial conditions can be expressed as in (23) [13], [42].

$$ L\{{}_{a}D_{t}^{\pm\alpha}f(t)\} = s^{\pm\alpha} \cong s^{\lambda}F(s), \quad 0 < \lambda < 1 \quad (23)$$

The difference between PI control and FOPI control is λ, whish is a fraction rather than integer. Provided that λ is positive for differentiation and negative for integration, FOPI control is calculated as in (24).

$$ G(s) = \frac{u(s)}{e(s)} = K_p + \frac{K_i}{s^{\lambda}} \quad (24)$$

where, G(s), u(s) and e(s) are rational functions of the variable s, Kp is a proportional control and Ki is an integral control.

4. Simulation Results and Discussions

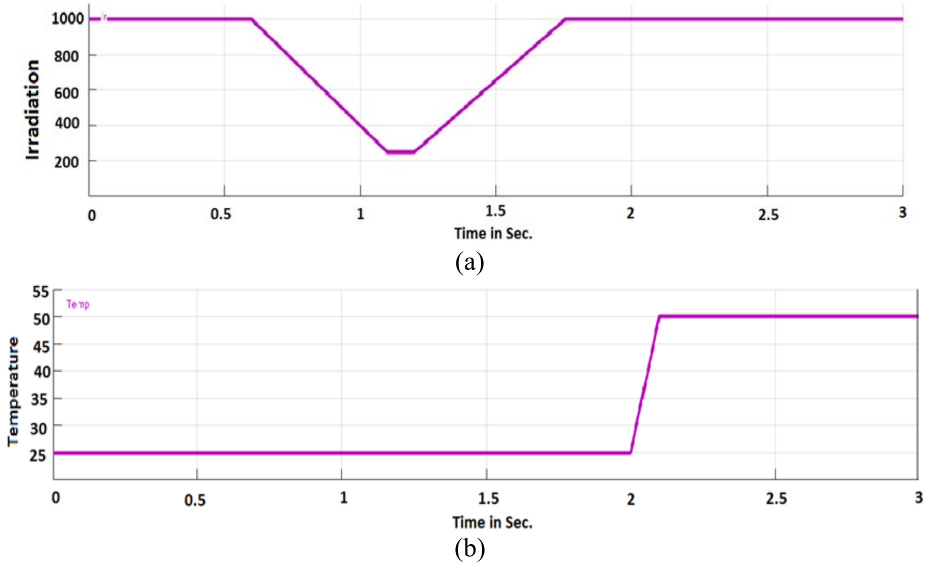

Figure 8. Weather condition [(a) Changing irradiation for PV (b) Changing Temperature for PV array]

To prove the effectiveness of the developed controllers, the next simulations are done under the changes in Figure. 8 and 9, which in turn affect to the output of power, current and power. Figure. 8 and 9 demonstrate the operating change of the irradiation and temperature in PV module and wind speed, respectively. All simulation and controllers' parameters are given table 1in the appendix. The next simulations are carried out via MATLAB/Simulink environment at two sides, namely, at the resources side and at the grid side.

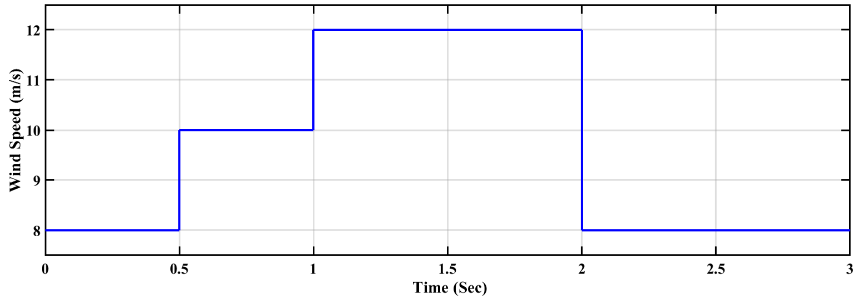

Figure 9. Wind profile for wind turbine.

A. Results at Resources Side

Considering the system demonstrated in Figure. 1, the PV currents are shown in Figure. 10 for FOPI, FIC, and classical PI controllers, respectively. The developed FOPI gives satisfactory results regarding the delivered PV current. The current from battery storage is illustrated in Figure. 11. The IC controller shows the worst performance. The battery current is steadier with the developed FOPI, which exhibits the satisfactory results. At time equals 2s, the PV temperatures increases from 25°C to 50°C, the classical PI lasts about 0.5s to restore the battery current and system stability at 2.5s. It is clear that the FOPI gives the shortest rise time with satisfactory overshoot compared to PI and FIC controllers and thus its effectiveness was affirmed.

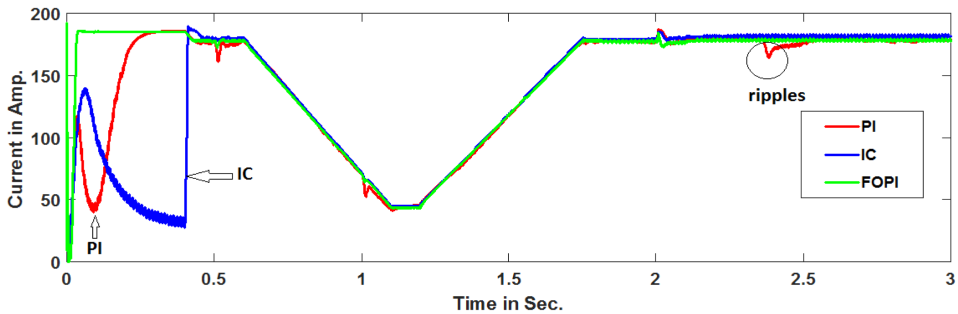

Figure 10. PV current in three types of control.

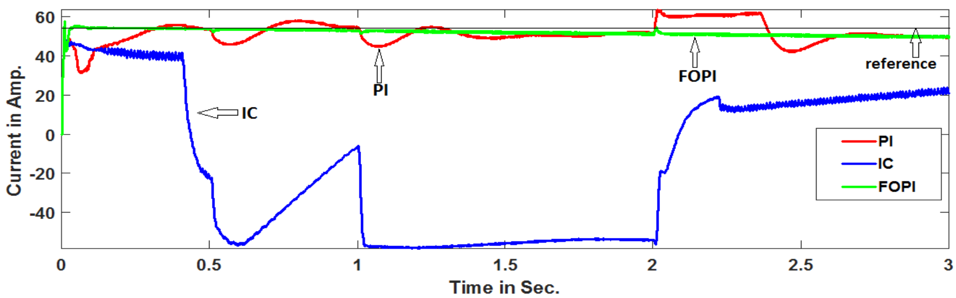

Figure 11. Battery storage current in three types of controller.

The wind turbine PMSG d- and q-axis stator currents are shown in Figure. 12 a and b for the developed controllers, respectively. At 1s, the wind speed experiences a step increase but solar irradiance continues to decrease. The IC controller demonstrates the worst performance with unsatisfactory frequency oscillations. The classic PI shows longer settling time with unsatisfactory overshoots and longer settling time (about 0.5s). The developed FOPI controller shows satisfactory transitions with the smallest ripples at the different weather disturbances results compared to FIC and PI controllers.

Figure 13 shows the PV output of power for the developed controllers. The wind turbine output power is shown in Figure. 14. Yet, the IC shows the worst performance. The developed FOPI controller gives acceptable results with diminished ripples to track reference line compared to the IC and PI controllers and its robustness was verified.

The battery powers are shown in Figure. 15. The IC shows unsatisfactory results at the long-term operating conditions. Initially, the PI shows longer settling time with limited over/undershoots compared to the FOPI. Still, the developed FOPI controller gives satisfactory results with the shortest settling time.

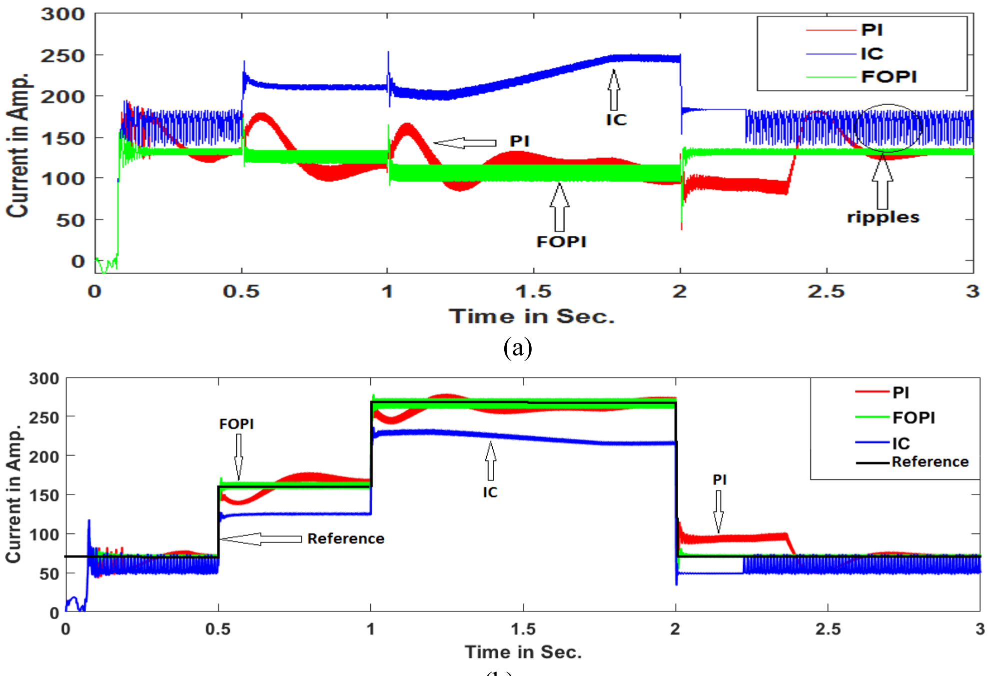

Figure 12. Stator current of wind turbine, (a) q-axis currents and (b) d-axis currents

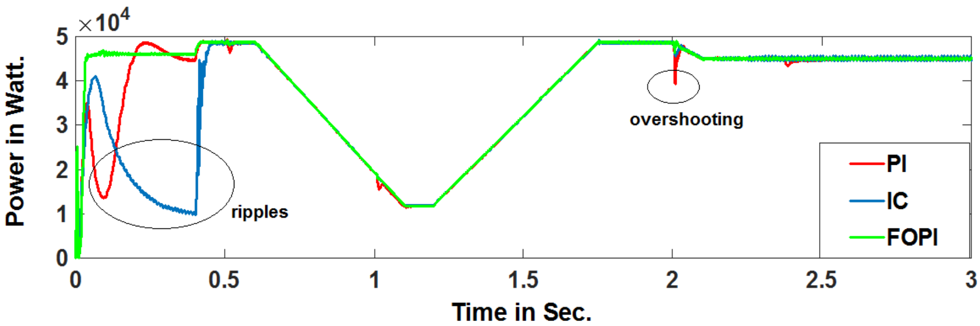

Figure 13. PV Output power.

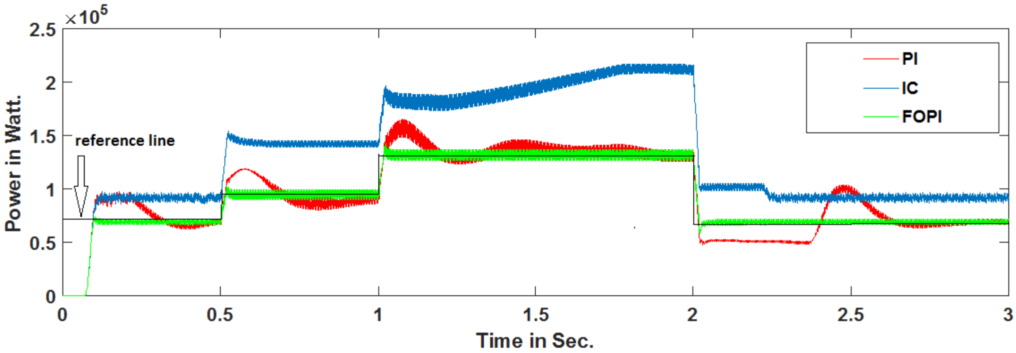

Figure 14. Wind turbine power from.

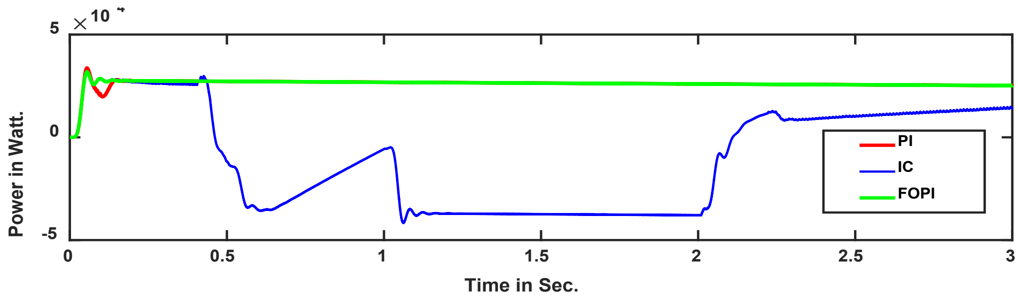

Figure 15. Battery storage output power.

B. Results at Grid Side

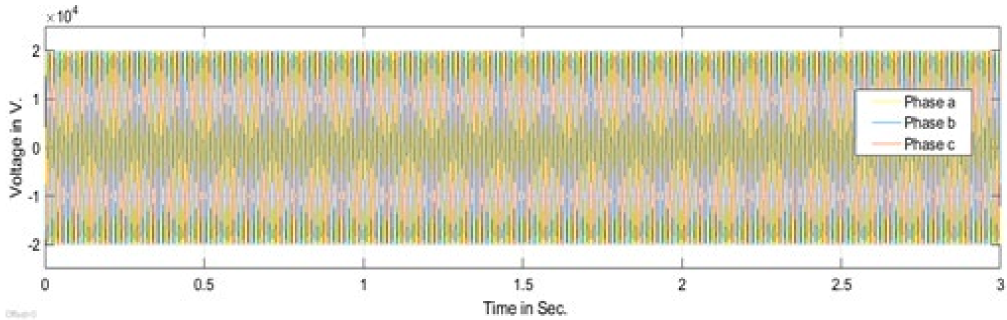

(a)

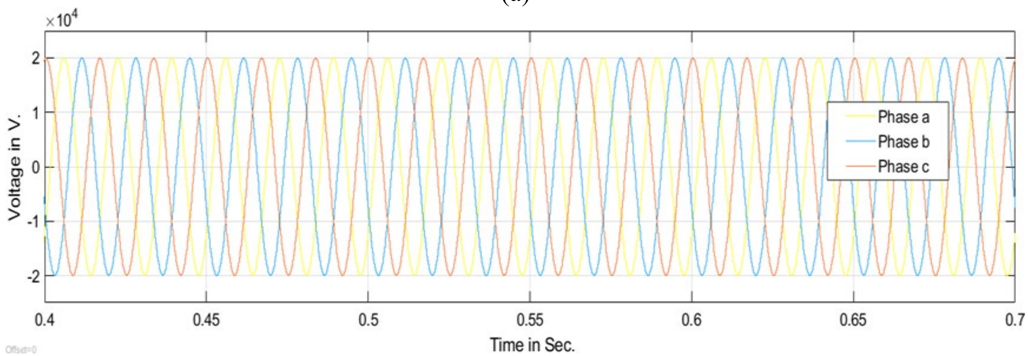

(b)

Figure 16. (a) Utility grid voltages profile and (b) Zoomed in Utility grid voltages profile

The inverter output voltage to the three-phase grid is illustrated in the Figure. 16.a and b. The grid injected current via the developed controllers is shown in Figures. 17, 18 and 19, respectively. Compared to the classical PI and IC, the developed FOPI exhibits satisfactory performance in terms of overshoots. Based on the result in Figure.19, FOPI gives the satisfactory performance, when it compared to other controllers. The FOPI controller responds quickly for the operation of inverter without ripples. Yet, FIC supplies lower current to the utility grid than other controllers, which results in smaller power delivered to the grid. IC demonstrates bad performance compared two other controllers.

The d-axis grid injected current is shown in Figures. 20. The classic PI controller tracks the reference current but at the cost of the settling time. Still the IC shows unsatisfactory results at the steady state and transient conditions. The developed FOPI shows adequate results to track the reference current and its robustness was proved.

The grid injected power via the developed PI, FOPI and IC controllers are allowed 85 kw, 86 kw and 65 kw as shown in Figure. 21. The FOPI responds satisfactorily for all changes of the wind speed and solar irradiation. However, the IC shows unsatisfactory results since it doesn't respond well for the wind speed and the irradiation changes.

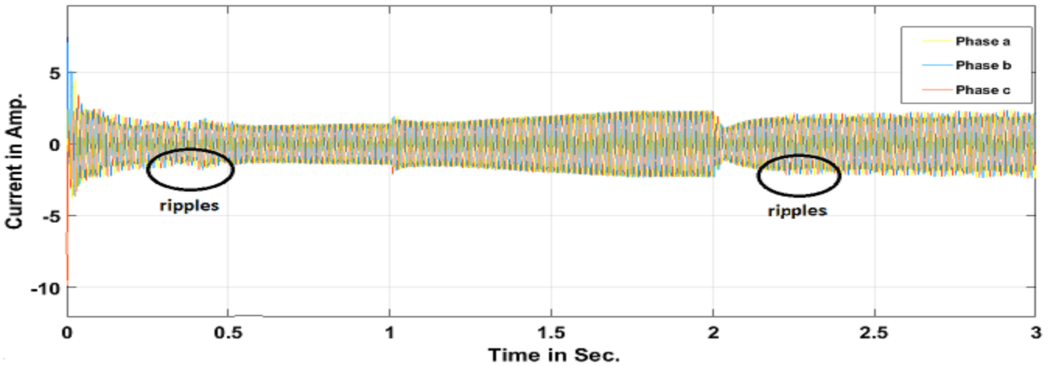

Figure 17. Grid injected current the using FIC.

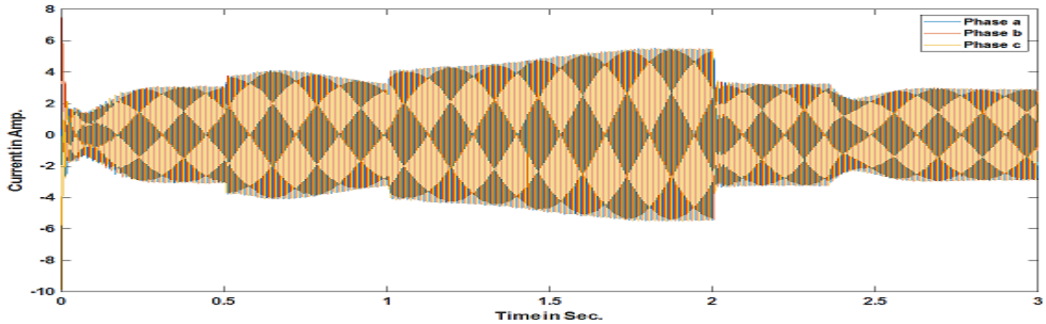

Figure 18. Grid injected t current using PI controller.

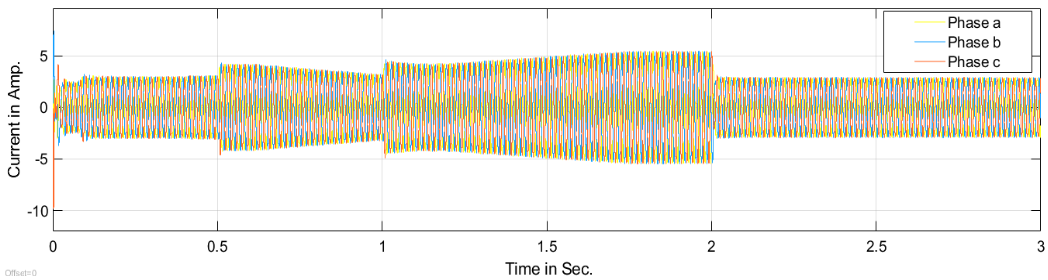

Figure 19. Grid injected current using FOPI controller.

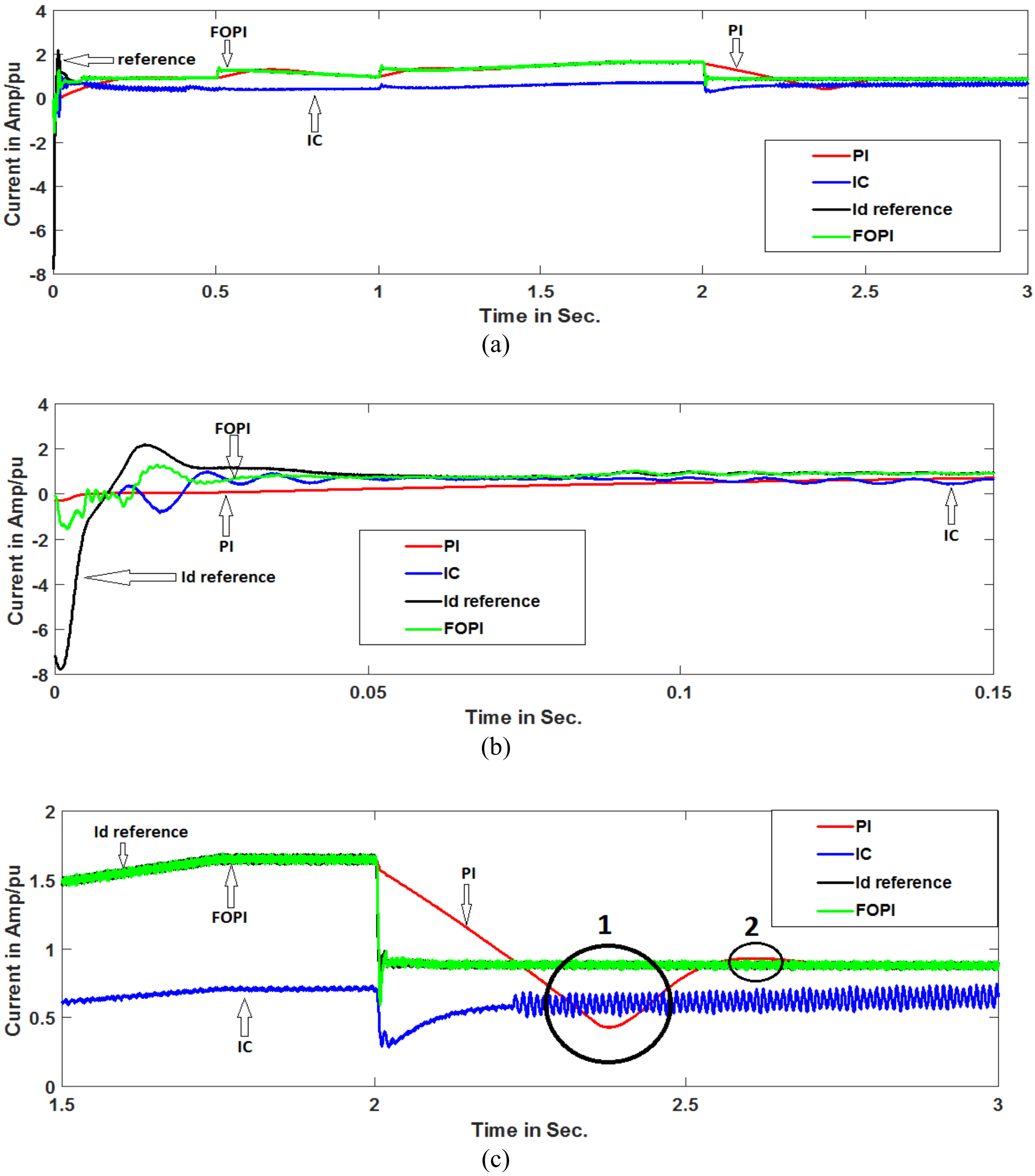

Figure 20. (a) Injected current control, (b) Zoomed in injected current control during the first 0.15s and (c) Zoomed in injected current control at last 1.5s.

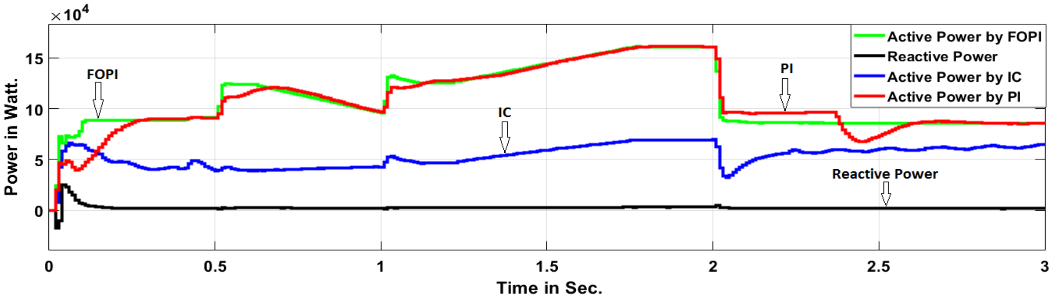

Figure 21. Grid injected power using the developed controller techniques.

5. Experimental Setup of PV-Wind Hybrid System

The data and description of the experimental system are presented table 2 in the appendix. As shown in Figure. 22, the experimental setup of a PV- wind hybrid system connected to the grid. The system consists of four busbars, the first busbar connected to the grid, the second busbar connected with loads, the third busbar connected with wind and the fourth busbar connected with PV.

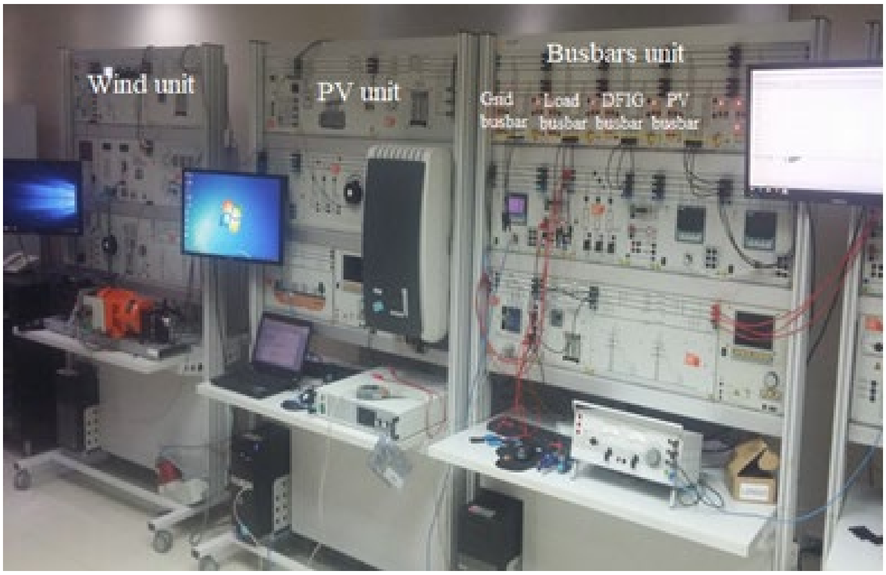

Figure 22. PV- wind hybrid system with experimental work.

Figure 23 shown, the step wind speed profile varies up and down as step functions with an average value of 10 m/s with duration of 60 s.

Figure 24 shows and illustrates the change of solar radiation under the ramp profile. We observe in the form of solar radiation starting from 325 W/m^2 and gradually rise to 675 W/m^2 and then dome slightly and then the radiation gradually decreases up to 260 W/m^2, then stability slightly, then gradually increase to 470 W/m^2 and then stability slightly.

Figure 25 shows the experimental performance of PV voltage, PV current and PV power under ramp changes of solar radiation.

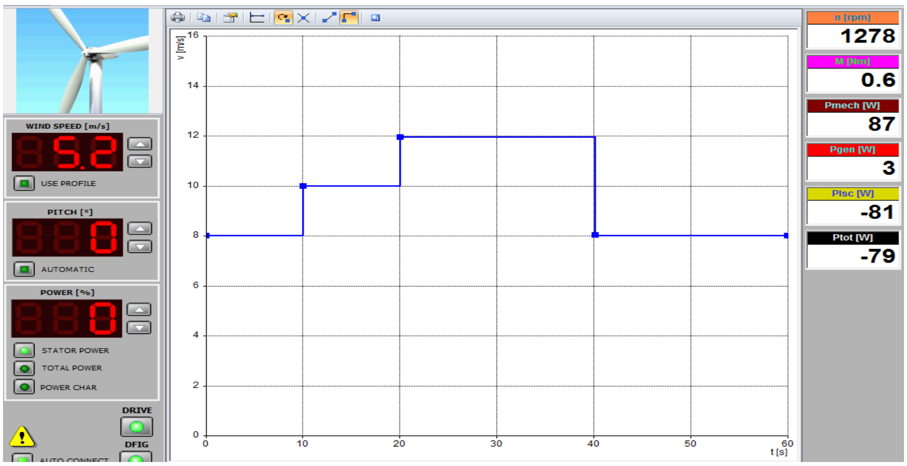

Figure 23. Wind speed profile in m/s of experimental wind energy.

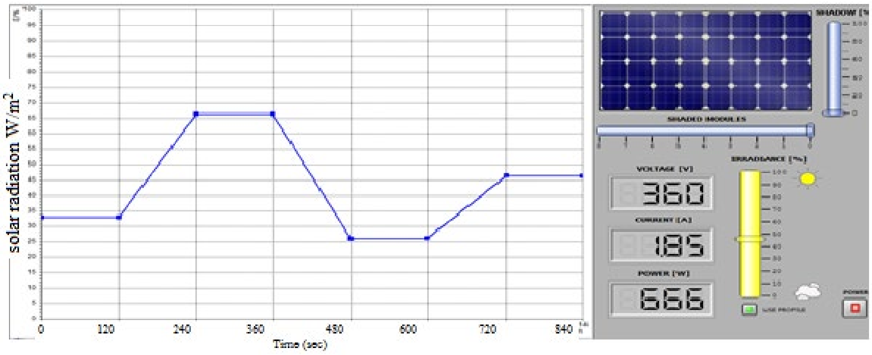

Figure 24. Ramp changes of solar radiation of experimental PV system.

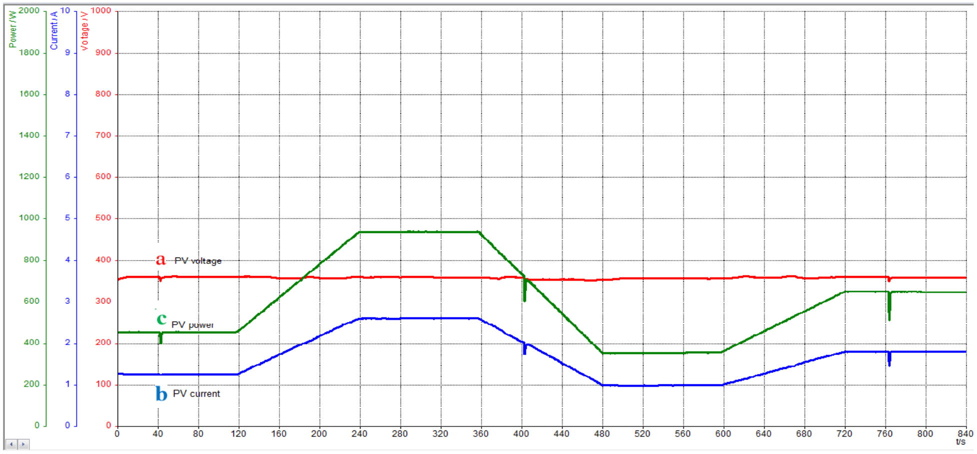

Figure 25. Experimental performance of PV voltage, PV current and PV power.

As shown in Figure. 26, the experimental performance of stator voltage in volt and stator current in ampere of wind energy. Figure 26 shows a constant voltage approximately, with a change in current, followed by a change in the wind speed.

The experimental performance of rotational wind speed of the wind generator in rpm and mechanical power in watt for wind energy, as seen in Figure 27.

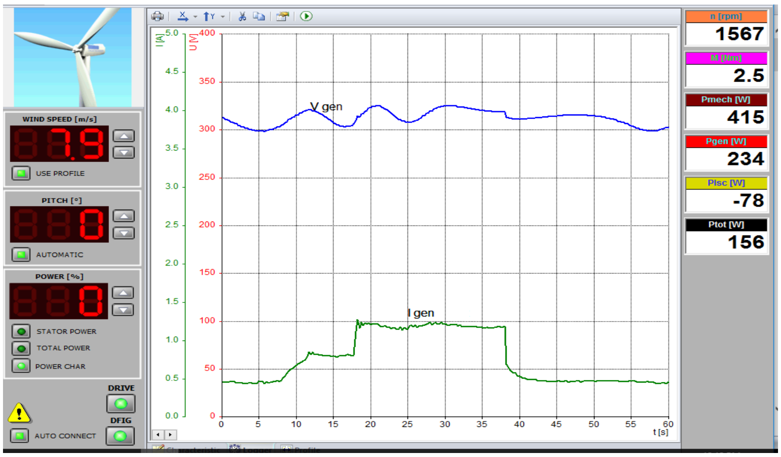

Figure 26. Experimental performance of stator voltage in volt and stator current in ampere of wind energy.

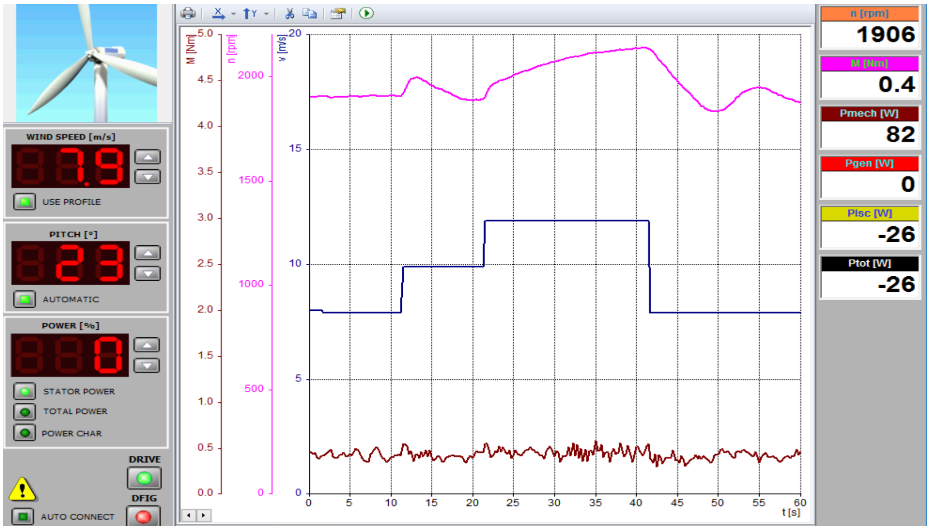

Figure 27. Experimental performance of rotational speed of the generator in rpm and mechanical power in watt.

Figure 28, describes the experimental performance of active, reactive and apparent wind power injected to the grid in watt for wind energy. A stability in the reactive power on the zero, with a change in the active power, followed by a change in the wind speed as shown in Figure. 28.

At any variation in wind speed, whether increased or decreased, followed by a similar variation in the mechanical torque and stability in the pitch angle on the zero, for the experimental response as exposed in Figure 29.

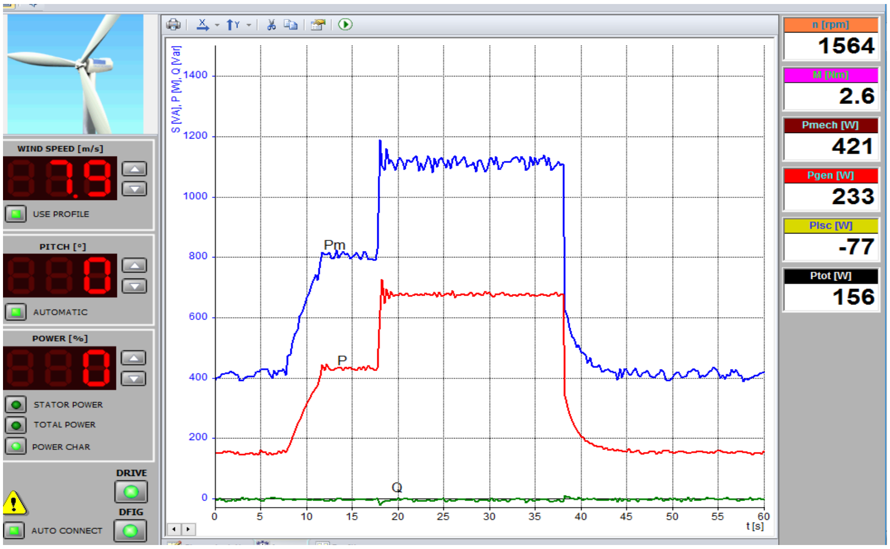

Figure 28. Experimental performance of active, reactive and apparent wind power injected to the grid in watt

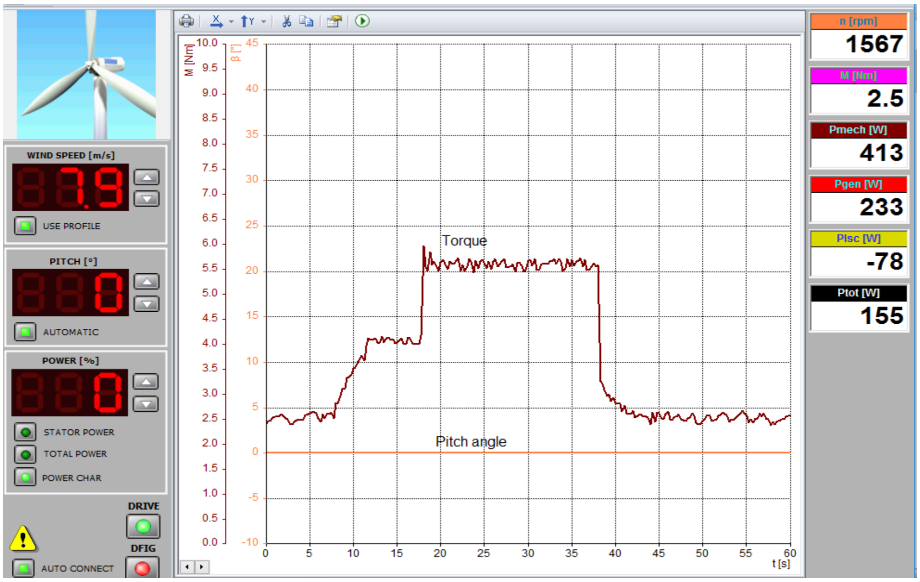

Figure 29. Experimental performance of input mechanical torque in Nm and pitch angle.

In Figure 30, it displays the results of the output power between the solar system and the wind energy connected to the grid. The output power of the wind energy was equivalent to 267 watts, while the output power of the solar energy equals 656 watts, so that the total grid connected power is 903 watts, as shown in Figure 30. In order to implement synchronization to the grid, three conditions must be same the phase sequence, grid voltage magnitude and frequency.

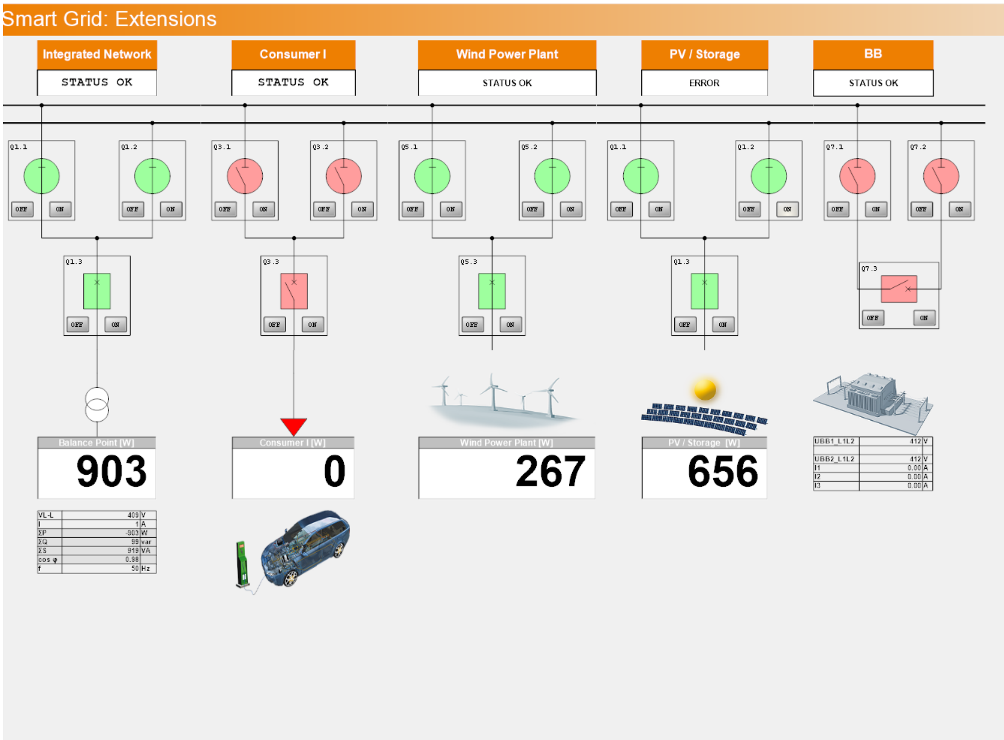

Figure 30. Experimental power results of PV – wind hybrid system connected to the grid.

6. Conclusion

This paper introduced a hybrid PV, wind turbine and battery storage system connected to a three-phase grid. In this research is compared three types of controller PI, FIC and FOPI. The effectiveness of the FOPI was demonstrated by a fair comparison with classic PI and IC. Based on digital simulation results, the following conclusions are drawn, (1) FOPI controller offers satisfactory performance to handle the power supplied to the grid, (2) FOPI can pave the way forward for more hybrid systems performance and different operating conditions, (3) IC by itself could not stabilize the system, (4) the HRES presented in this study is considered as an initial step to enhance the power provided to the grid, (5) it seems that the solar irradiation and wind speed variations have more impact upon the power delivered to the grid than the PV ambient temperature. Thus, the current word recommends utilizing the developed FOPI for future works. For the purpose of future works, techno-economic feasibility analysis could be estimated to discover the optimal size and configuration of the individual components. Furthermore, experimental analysis is to be done to highlight the stability analysis.

Through experimental results, the synchronization process between the wind energy system with PV energy and the electrical grid was verified. The results of the performance of the PV / wind synchronization with the grid are presented. It was also presented the results of the current and voltage and power PV / wind with the grid in addition to the torque-speed for standalone wind energy.

Appendix

Table 1. Simulation System Parameters.

Parameter	Value
PV Parameters	
PV maximum power of module	305.23 W
PV open circuit voltage of module	64.2 V
PV short circuit current of module	5.96 A
PV maximum voltage of module	54.7 V
PV maximum current of module	5.58 A
Parallel strings of PV array	66
Series-connected modules per string	5
Inductance of boost converter	5e-3 H
Resistance of boost converter	0.005 Ώ
Capacitance of boost converter	100e-6 F
Total P_{PV} Array	45KW
Wind Parameters	
Mechanical of Wind output power	200000 W
Base wind speed	12 m/s
Maximum power at base wind speed	0.8 pu
Base power of the electrical generator	200000/0.9 VA
Pitch angle beta	0 deg
Resistance of Rectifier	100 Ohms
Capacitance of Rectifier	0.1e-6 F
P_{wind}	69.7KW
Battery Parameters	
Nominal voltage of Battery	300 V

Rated capacity	6.5 Ah
$P_{Battery}$	22KW
Grid Parameters	
Step up transformer	260V / 25 kV
Grid voltage	20000 V
Grid frequency	60 Hz
Controller Parameters	
Kp Current Control at PI	0.3
Ki Current Control at PI	20
Kp Voltage Source Control at PI	7
Ki Voltage Source Control at PI	800
Reference voltage of DC link	500 V
P_{out} at PI	85.35 KW
P_{out} at FOPI	86 KW
P_{out} at IC	65 KW
λ at FOPI	0.8

Table 2: Experimental setup specifications

Names	Values
PV array	
PV maximum power	1500 W
Rated current	7.2 – 11.7 A
Rated voltage	100 - 240 V
Output current	0-10 A
Output voltage	0-500 V
ON-grid inverter	
DC input voltage	250 – 1000V
DC MPP Voltage	300 – 800V
DC Max. current	11 A
DC Short circuit current	13 – 20 A
AC voltage	3*230 V
Frequency	50-60 HZ
Power Factor	0.8 – 1.0
AC Max. Current	7 A
Max. Power	3200 W
Step up transformer	
Primary Voltage	400 V
Secondary Voltage	450 V
Nominal Power	1000 VA
Frequency	50/60 HZ
Length of transmission line	150 km
Wind Energy	
Wind Unit	0.8 kW, 50 Hz, 230/400 V
Servo machine	Nominal speeds 2000 rev/min, T=6.7 N.m
Incremental encoder	6000 rpm, 1024 pulses, Moment of inertia: 35 gcm^2

7. References

[1]. A. Tjahjono, D. O. Anggriawan, M. N. Habibi, and E. Prasetyono, "Modified Grey Wolf Optimization for Maximum Power Point Tracking in Photovoltaic System under Partial Shading Conditions, "*International Journal on Electrical Engineering and Informatics (IJEEI),* vol. 12, no. 1, March 2020.

[2]. D. K. Lal1, B. B. Dash, and A. K. Akella, "Optimization of PV/Wind/Micro-Hydro/Diesel Hybrid Power System in HOMER for the Study Area," *International Journal on Electrical Engineering and Informatics (IJEEI)*, vol. 3, no. 3, 2011.

[3]. W. A. Mirza, H. Sheh Zad and S. Bashir, "Robust and Optimal Maximum Power Point Tracking Control of Solar PV Power System," 2020 *3rd International Conference on Computing, Mathematics and Engineering Technologies*, Sukkur, Pakistan, pp. 1-6, 2020.

[4]. F. K. Abo-Elyousr, and A. Elnozahy, "Bi-objective economic feasibility of hybrid micro-grid systems with multiple fuel options for islanded areas in Egypt," *Rene. Energy*, vol. 128(1), pp. 37-56, 2018.

[5]. C. M. Nirmal Mukundan, P. Jayaprakash, U. Subramaniam and D. J. Almakhles, "Binary Hybrid Multilevel Inverter-Based Grid Integrated Solar Energy Conversion System with Damped SOGI Control," *IEEE Access*, vol. 8, pp. 37214-37228, 2020.

[6]. K. Anoune, M. Bouya, M. Ghazouani, A. Astito, and A. Ben Abdellah, "Hybrid renewable energy system to maximize the electrical power production," *Int. Renew. Sustain. Energy Conf.*, pp. 533–539, 2016.

[7]. A. M. Yousef, M. Ebeed, F. K. Abo-Elyousr, A. Elnozohy, M. Mohamed and S. A M. Abdelwahab "Optimization of PID Controller for Hybrid Renewable Energy System Using Adaptive Sine Cosine Algorithm," *International Journal of Renewable Energy Research-IJRER*, pp 670-677, vol 10, no 2, 2020.

[8]. M. Prodanovic, and T. C. Green, "Control and filter design of three-phase inverters for high power quality grid connection," *IEEE. Personal use of this material is permitted*, 2003.

[9]. R. Hilfer, Applications of Fractional Calculus in Physics. Word Scientific, Singapore, 2000.

[10]. C. Tseng and S. Lee, "Designs of Fixed-Fractional-Delay Filters Using Fractional-Derivative Constraints," in *IEEE Transactions on Circuits and Systems II: Express Briefs*, vol. 59, no. 10, pp. 683-687, Oct. 2012.

[11]. B. P. Ga, S. Mohanty, P. K. Rana, and Preeti Kum, "Compensation of voltage sag using DVR with PI controller," *Int. Conf. (ICEEOT)*, India, 2016.

[12]. I. Putri, A. Rizqiawan, T. D. Rachmildha, Y. Haroen, and P. A. Dahono, "Minimization of Dead-Time Effect in Current-Controlled Three-Phase PWM Inverters by Using Virtual Inductor" *International Journal on Electrical Engineering and Informatics (IJEEI)*, Vol. 12 No. 1, March 2020.

[13]. F. K. Abo-Elyousr, and A. M. Sharaf, "A novel modified robust load frequency controller scheme," Energy Systems, Springer-Verlag GmbH Germany, part of Springer Nature, pp. 1-24, 2019.

[14]. A. Kumar, K. N. Mustikovila, G. K. Singh, S. Lee, and H. N. Lee, "A new design method for FIR notch filter using Fractional Derivative and swarm intelligence," Sādhanā, vol. 44(3), pp. 61, 2019.

[15]. V. A. Kumar, and A. Mouttou, "Improved performance with fractional order control for asymmetrical H-bridge multilevel inverter," *Bulletin of Electrical Engineering and informatics*, vol. 9, pp. 1335-1344, 2020.

[16]. N. Shafaghatian, A. Kiani, N. Taheri, Z. Rahimkhani, and S. S. Mascoumi, "Damping controller design based on FO-PID-EMA in VSC HVDC system to improve stability of hybrid power system," *J. Cent. South. Univ.*, vol. 27, pp. 403-417, 2020.

[17]. A. Narendran, and R. Sureshumar, "Hysteresis-controlled-landsman converter based multilevel inverter fed induction-motor system using PIC," Microprocessors and Microsystems, vol. 76, pp. 103099, 2020.

[18]. A. Rawat, S. K. Jha, B. Kumar, and V. Mohan, "Nonlinear fractional order PID controller for tracking maximum power in photo-voltaic system," *Journal of Intelligent & Fuzzy Systems, (Preprint)*, pp. 1-24, 2020.
[19]. K. Farjami, A. Mohammadzadeh, A. Ahmadian, and S. Shoja, "Designing a fuzzy PI^ lambda controller to control the pitch angle in wind turbines under variant speed," Iranian Electric Industry Journal of Quality and Productivity, vol. 9(1), pp.1-15, 2020.
[20]. B. Puchalski, A. R. Tomasz, and D. Kazimierz, "Fuzzy Multi-Regional Fractional PID controller for Pressurized Water nuclear Reactor," ISA transactions [In press], 2020.
[21]. Z. Qi, H. Yang, M. Li, and J. Li, "Research on Fractional Order PID Controller in Servo Control System" In 2019 *IEEE 3rd Conference on Energy Internet and Energy System Integration (EI2)*, vol. 1, pp. 2931-2935, 2019.
[22]. F. Meng, S. Liu, and K. Liu, "Design of an Optimal Fractional Order PID for Constant Tension Control System. *IEEE Access*, vol. 8, pp. 58933-58939, 2020.
[23]. O. W. Abdulwahhab, and N. H. Abbas, "Survey Study of Factional Order Controllers," *Journal of Engineering*, vol. 26(4), pp. 188-201, 2020.
[24]. J. Z. Shi "A Fractional Order General Type-2 Fuzzy PID Controller Design Algorithm," *IEEE Access*, vol. 8, pp. 52151-72, 2020.
[25]. Zaheeruddin, and K. Singh, "Intelligent Fractional-Order-Based Centralized Frequency Controller for Microgrid," *IETE Journal of Research*, pp. 1-15, 2020.
[26]. R. P. Naidu, and S. Meikandasivam, "Power quality enhancement in a grid-connected hybrid system with coordinated PQ theory & fractional order PID controller in DPFC," *Sustainable Energy, Grids and Networks*, pp. 100317, 2020.
[27]. K. Dziedzic, "Tuning the Fractional Order PID Controller in the Forced Air Heating System Using Biologically Inspired algorithms," *In Conference on Automation*, vol. 146, pp. 135-146, Springer, Cham, 2020.
[28]. Y. Q. Guo, J. Zhang, D. Q. He, and J. B. Li, "Magnetorheological Elastomer Precision Platform Control Using OFFO-PID Algorithm," *Advances in Materials Science and Engineering*, 2020.
[29]. A. K. Patra, A. K. Mishra, and R. Agrawal, "Fractional Order PID Controller Design for Stabilizing and Trajectory Tracking of Vehicle System," *Innovation in Electrical Power Engineering, Communication, and Computing Technology*, Springer, Singapore, vol. 1, pp. 595-607, 2020.
[30]. M. S. Bouakkaz, A. Boukadoum, O. Boudebbouz, N. Fergani, N. Boutasseta, I. Attoui, A. Bouraiou, and A. Necaibia, "Dynamic performance evaluation and improvement of PV energy generation systems using Moth Flame Optimization with combined fractional order PID and sliding mode controller," *Solar Energy*, vol. 199, pp. 411-424, 2020.
[31]. A. Elnozahy, A. K. Abdel-Rahman, A. Hamza, H. Ali, M. Abdel-Salam, and S. Ookawara "Thermal/electrical modeling of a PV module as enhanced by Surface Cooling", *Journal of Clean Energy Technologies*, vol. 4, no. 1, January 2016.
[32]. M. O. Abdel-Raouf, M. I. Mosaad, and A. Mallawany, "MPPT of PV-wind-fuel cell of off-grid hybrid system for a new community" Twentieth International Middle East Power Systems Conference (MEPCON), Cairo University, Egypt, 2018.
[33]. S. S. Dessouky, A. A. Elbaset, A. H. K. Alaboudy, H. A. Ibrahim and S. A. M. Abdelwahab, "Performance improvement of A PV-powered induction-motor-driven water pumping system," 2016 *IEEE International Middle-East Power Systems Conference (MEPCON)*, Helwan University, Egypt, December 27-29, 2016.
[34]. J. Yoo, J. Kim; J. Park "Converter control of PMSG wind turbine system for inertia-free stand-alone microgrid" *IEEE Industry Applications Society Annual Meeting*, pp. 1-8, 2016.
[35]. N.S. Jayalakshmi and D.N. Gaonkar, "A New Control Method to Mitigate Power Fluctuations for Grid Integrated PV/Wind Hybrid Power System Using Ultra capacitors", *International Journal of Emerging Electric Power Systems*, vol. 17, no. 4, pp. 451-461, 2016.

[36]. L. Wang, S. Sharkh, and A. Chipperfield, "A-Based optimal coordination of vehicle-to-grid batteries and renewable generators in a distribution network," *IEEE 26th International Symposium on Industrial Electronics (ISIE)*, 2017.
[37]. S. S. Dessouky, W. S.E. Abdellatif, S. A. M. Abdelwahab and Marwa A. Ali, "Maximum Power Point Tracking Achieved of DFIGURE-Based Wind Turbines Using Perturb and Observant Method," *IEEE International Middle-East Power Systems Conference*, December 18-20, 2018.
[38]. A. A. Elbaset, S. A. M. Abdelwahab, H. A. Ibrahim and M. A. E. Eid "Performance Analysis of Photovoltaic Systems with Energy Storage Systems," *Renewable and Green Energy*, Springer, January 2019.
[39]. A. H. K. Alaboudy, A. A. Elbaset and S. A. M. Abdelwahab, "Effect of dc link capacitance on stand-alone PV system operation with fluctuated dc resistive loads," *Port -Said Engineering Research Journal*, vol. 19, no. 1, pp. 121-128, March 2015.
[40]. A. M. Eltamaly, Y. S. Mohamed, A. N. Abd-Elghaffar, and A. M. El-Sayed, "Enhancement of power system quality using PI control technique with DVR for mitigation voltage sag", *Twentieth International Middle East Power Systems Conference (MEPCON)*, Cairo University, Egypt, 2018.
[41]. M. A. E. Eid, S. A. M. Abdelwahab, H. A. Ibrahim and A.H. K. Alaboudy "Improving the Resiliency of a PV Standalone System Under Variable Solar Radiation and Load Profile," *IEEE International Middle-East Power Systems Conference*, December 18-20, 2018.
[42]. Saad A M. Abdelwahab, Walid S.E. Abdellatif, and Abdallah Mohamed Hamada, "Comparative Analysis of the Modified Perturb & Observe with Different MPPT Techniques for PV Grid Connected Systems," *International Journal of Renewable Energy Research-IJRER*, pp 156-164, Vol 10, No 1, 2020.
[43]. R. Ranganayakulu, G. U. B. Babu, A. S. Rao, and D. S. Patle, "A comparative study of fractional order PIλ/PIλDμ tuning rules for stable first order plus time delay processes," ScienceDirect, *Resource-Efficient Technologies* 2, S136–S152, 2016.
[44]. M. A. E. Eid, A. A. Elbaset, H. A. Ibrahim and S. A. M. Abdelwahab, "Modelling, Simulation of MPPT Using Perturb and Observe and Incremental Conductance techniques For Stand-Alone PV Systems," 2019 21st *International Middle East Power Systems Conference (MEPCON)*, Cairo, Egypt, pp. 429-434, 2019
[45]. B. Shang, J. Liu, T. Zhao, and Y. Chen, "Fractional order robust visual Servoing Control of a Quadrotor UAV with Larger Sampling Period," *International Conference on Unmanned Aircraft Systems (ICUAS)* June 7-10, 2016. Arlington, VA USA, 2016.

Ali Mohamed Yousef, born in 1968. He received B.Sc. degree from Faculty of Engineering, Assiut University, Egypt, in 1993. He received his M. Sc. and Ph.D. from the Department of Electrical Power and Machines, Faculty of Engineering, Assiut University, Assiut, Egypt, in 1998 and 2003, respectively. He gets an Associate Professor 2008. Now he is a Professor of power system control since May 2014. Scientific area research is renewable energy, power electronics, drives, power system control, Fuzzy control, Robust Control.

Farag K. Abo-Elyousr was born on Assiut on January 1978. He got his M. Sc and Ph. D. degrees from Assiut University on 2000 and 2015, respectively. During his previous M. Sc and Ph. D., he developed many DC/DC and DC/AC power supplies prototypes for various fields such as battery and supercapacitor charging purposes. Also, he worked in electric vehicle power electronics modeling, developing, and testing. His M. Sc. was related to electric machines and its related topics such as AC drives. However, his Ph. D. thesis was related to electric propulsion systems. He had a teaching experience increases than 20 years. During this period of education, he published many theoretical and experimental research articles. He also co-worked in many research projects. Currently, his research interests include power system optimization and control in the context of microgrids, power electronics, and stability issues.

Ahmed Elnozahy was born in Sohag, Egypt, on January 1, 1979. Elnozahy got the degree of Master of Science in Electrical Engineering from Assiut University in April 2013 and Ph. D. degree in Energy Resources Engineering from Egypt-Japan University of Science and Technology (E-JUST) in Sept. 2016. Currently, Elnozahy is an Assistant Professor in Electrical Engineering Department at Assiut University. His research interests are renewable energy, particularly, photovoltaic energy, wind energy, solar energy, fuel cells applications, and optimization of hybrid renewable energy systems.

Moayed Mohamed received the B.S. from Faculty of Industrial Education, Sohag University, Sohag, Egypt, in 2014 and M.Sc. from Faculty of Industrial Education, Suez University, Suez, Egypt in 2017. Now working at Ph.D. from Faculty of Industrial Education, Electrical Department, Sohag University, Egypt. During 2015 to 2017 he was a demonstrator at Faculty of Industrial Education, Sohag University, Sohag, Egypt. He is assistant lecture in Electrical Department (Power & Machines Section), Faculty of Industrial Education, Sohag University, Sohag, Egypt since 2017 until now days. His research interests are in the area of Renewable energy sources, Control theory and applications and optimization techniques.

Saad A. Mohamed Abdelwahab received the B.S. from Faculty of Industrial Education, Suez Canal University, Suez, Egypt, in 2006 and M.Sc. from Faculty of Industrial Education, Suez Canal University, Suez, Egypt in 2011 and Ph.D. from Faculty of Industrial Education, Electrical Department, Suez University, Egypt, 2016. During 2007 to 2010 he was a demonstrator at Faculty of Industrial Education, Suez Canal University, Suez campus, Suez, Egypt. He is assistant lecture in Electrical Department (Power & Machines Section), Faculty of Industrial Education, Suez University, Suez, Egypt since 2011 until 2015. He is a member of Faculty of Technology and Education, Suez University, Suez, Egypt form 2016. Currently, his research interests are in the area of renewable energy sources, power electronics, power system optimization, high voltage and power quality.